THE ASTROPHYSICAL JOURNAL, 396:730–740, 1992 September 10

SPATIAL HETERODYNE SPECTROSCOPY FOR THE EXPLORATION OF DIFFUSE INTERSTELLAR EMISSION LINES AT FAR-ULTRAVIOLET WAVELENGTHS

J. HARLANDER,[1] R. J. REYNOLDS, AND F. L. ROESLER[2]
Department of Physics, University of Wisconsin-Madison, 1150 University Avenue, Madison, WI 53706
Received 1991 August 19; accepted 1992 March 12

ABSTRACT

Spatial heterodyne spectroscopy (SHS) is a new instrumental technique for interference spectroscopy which promises to extend into the FUV (1200–2000 Å) spectral region the large throughput advantage at high spectral resolution usually associated with Fabry-Perot and Michelson interferometers. In addition, SHS systems are compact in size, can be field-widened to increase their throughput advantage even further, have no moving parts, and can be built in all-reflection configurations. SHS appears to be well suited for high resolution, space-based spectroscopy of faint interstellar emission lines in the ultraviolet. This has significant implications for the study of the dynamics and distribution of hot gas within the Galactic disk and halo. For example, a field-widened SHS incorporating 5 × 5 cm gratings could obtain a radial velocity resolved (20 km s^{-1}), 3° angular resolution map of the high-latitude interstellar C IV λ1550 emission in less than 1 year. SHS systems built and tested in the laboratory at visible and UV (2500 Å) wavelengths have verified the basic concepts and performance characteristics of the technique, and the development of SHS for FUV astrophysics has begun.

Subject headings: instrumentation: spectrographs — ultraviolet: interstellar

1. INTRODUCTION

Interference spectrometers, such as Fabry-Perots and Michelsons, offer significant advantages over conventional grating spectrometers in the study of faint, spatially extended sources (e.g., Roesler 1974). The primary advantages are (1) an étendue, or throughput, typically 200 times larger than grating spectrometers operating with a similar spectral resolution and dispersing element area; (2) compact size, especially at high resolution; and (3) relative ease of attaining high spectral resolution. In combination these advantages can provide scientific programs with important economies in observing time, cost, weight, and volume. They also can make accessible for detailed exploration extended sources that are too faint to be studied by the more conventional techniques. For example, Fabry-Perot spectrometers have made it possible to study the distribution, kinematics, and ionization conditions of the warm (10^4 K) ionized component of the interstellar medium, a major component of the medium that is accessible through its very faint line emission at optical wavelengths (Roesler et al. 1978; Reynolds 1990; Reynolds et al. 1990). Michelson interferometers also play an important role, particularly at infrared wavelengths in the detection and study of faint emission lines from the cooler ($\gtrsim 10^3$ K) components of the interstellar medium.

If interference spectroscopy could be extended into the FUV ($1100 < \lambda \leq 2000$ Å) and EUV ($\lambda \leq 1100$ Å) spectral regions, it would profoundly impact studies of the *hot* (10^5–10^6 K) component of the interstellar medium (Roesler, Harlander, & Reynolds 1990). The individual, extremely faint emission lines from trace ions within the hot gas could be identified and mapped over the sky, and the line profiles could be resolved to provide detailed kinematic information. Such capabilities would address one of the most important questions in Galactic astronomy—the role played by hot gas in determining the overall structure and dynamics of interstellar matter (e.g., Cox 1989; McKee 1990).

Unfortunately, Fabry-Perot and Michelson spectrometers cannot be readily adapted to the FUV and EUV, where emission lines from the hot component are produced. This is due in part to the tolerance requirements at short wavelengths for both the optical surfaces and mechanical structures of such devices. Also, in the EUV optical materials are not available or of sufficient quality for interferometry. All-reflection Michelson FTS systems have been designed and tested (Kruger, Anderson, & Roesler 1972; Fonck et al. 1978), but the required scan and control mechanisms are complex and costly. Moreover, such systems are not adaptable to space-based astrophysical applications demanding instruments that are compact, lightweight, and robust.

At the University of Wisconsin a new interferometric technique, called spatial heterodyne spectroscopy (SHS), has been conceived (Harlander & Roesler 1990) and is being developed (Harlander 1991; Roesler & Harlander 1991; Harlander, Roesler, & Chakrabarti 1991), which brings the advantages of interference spectroscopy into the FUV and perhaps the EUV spectral regions. In a series of experimental and analytical studies, we have verified that spectrometers operating on the SHS principle do achieve the combination of high spectral resolution and large throughput associated with Fabry-Perots and Michelsons, and that they can be field-widened without any moving elements to increase their throughput even further. In this paper we describe the basic SHS concepts, present the results of new performance tests in the laboratory, and briefly discuss the planned application of SHS to the study of diffuse emission lines from 10^5 K gas in the interstellar medium.

2. THE TRANSMITTING SPATIAL HETERODYNE SPECTROSCOPY

We believe that SHS provides the first practical approach to interference spectroscopy in the ultraviolet. At the University of Wisconsin we have begun a program with support from

[1] New postal address: Department of Physics, St. Cloud State University, St. Cloud, MN 56301.
[2] Temporary postal address: Aeronomy Section, National Science Foundation, Washington, DC 20550.

NASA to develop a field-widened SHS incorporating transmitting optics for velocity-resolved studies of C IV λ1550, O III] λ1663, and other faint emission lines in the 1350–1950 Å spectral region produced by the 10^5 K component of the interstellar medium. The basic characteristics of this instrument are described below.

2.1. *The Basic Spatial Heterodyne Spectroscopy Concept*

SHS can be understood by considering the transmitting beamsplitter arrangement illustrated in Figure 1, where a conventional Michelson interferometer is shown with the return mirrors replaced by diffraction gratings G_1 and G_2. Light enters through aperture A_1 and is collimated by lens L_1. At the exit, lenses L_2 and L_3 relay the superposed coherent images of gratings G_1 and G_2 onto the image plane I where a position-sensitive detector records the Fizeau fringe pattern produced by the interferometer. The generation of Fizeau fringes of wavenumber-dependent spatial frequency follows from the grating equation:

$$\sigma[\sin\theta + \sin(\theta - \gamma)] = \frac{m}{d}, \quad (1)$$

where m is the order of diffraction, θ is the Littrow angle, $1/d$ is the grating groove density, and γ is the diffraction angle with respect to Littrow for light of wavenumber σ. For a monochromatic point source in the input aperture on axis, two coherent plane wavefronts are produced at the output (labeled 1 and 2 in Fig. 1) whose wavevectors are inclined to the optical axis by angles γ and $-\gamma$, respectively, as shown in Figure 2. If the magnification by L_2 and L_3 were unity, these crossed wavefronts would produce on the detector plane Fizeau fringes perpendicular to the x-axis with a spatial frequency along the x-axis given by

$$f_x = 2\sigma \sin\gamma \approx 4(\sigma - \sigma_0)\tan\theta, \quad (2)$$

where the right-hand side of equation (2) is derived from an expansion of equation (1) for small γ, and σ_0 is the Littrow ($\gamma = 0$) wavenumber. Therefore, for an arbitrary input spectral density $B(\sigma)$, the intensity recorded as a function of position x is given by

$$I(x) = \int_0^\infty B(\sigma)[1 + \cos\{2\pi[4(\sigma - \sigma_0)x\tan\theta]\}]d\sigma, \quad (3)$$

where x is measured on the detector in the dispersion plane of the gratings.

The Fourier transform of $I(x)$ recovers the input spectrum. In this process, no element is mechanically scanned and zero spatial frequency corresponds to $\sigma = \sigma_0$. Effectively, SHS records the Fourier transform of the spectrum on a position-sensitive detector without scanning, and heterodynes the interferogram with a frequency corresponding to the Littrow wavenumber of the gratings. Zero spatial frequency can be set at a selected wavelength, and thus the system is analogous to the more familiar temporal frequency heterodyne techniques.

The resolving power, $R \equiv \sigma/\delta\sigma$, can be shown to be equal to the theoretical resolving power of the dispersive (i.e., grating) system (Harlander 1991). For the geometry in Figure 1 the result is

$$R = 4W\sigma \sin\theta, \quad (4)$$

where W is the width of the gratings. As in Michelson FTS, the SHS resolving power is simply twice the maximum path difference in the system divided by the wavelength.

The spectral range of one-dimensional SHS systems is limited by the highest spatial frequency that can be recorded on the imaging detector without aliasing. For N detector elements in one dimension, $N/2$ spectral elements may be recovered. Note that the number of resolution elements recovered is independent of the resolution. This is a direct result of the heterodyned nature of the interferogram recorded by SHS systems, which enables them to attain high resolution over a narrow spectral range with relatively few samples.

By including off-axis input angles in the grating equation (eq. [1]) it can be shown that the change in spatial frequency $f_x(\sigma)$ with off-axis angle limits the usable solid angle field-of-view Ω of SHS instruments to $\Omega = 2\pi/R$ (Harlander 1991). This is the same value achieved by conventional FTS and Fabry-Perot interferometers.

An alternative approach to understanding the SHS concept is to consider the Fizeau fringes produced by a conventional Michelson interferometer aligned with the mirrors tilted with respect to the optical axis by equal and opposite angles. By imaging these fringes, a nonscanned Fourier transform of the spectrum can be obtained (Stroke & Funkhouser 1965). However, the spectral resolution of this system is limited by the maximum spatial frequency that can be recorded by a finite number of detector elements. In SHS the spatial frequencies are heterodyned by replacing the tilted mirrors with Littrow diffraction gratings. This reduces the fringe frequency seen at the detector while retaining high resolution and throughput.

In SHS and FTS systems all spectral elements contribute photons to every sample in the interferogram, and therefore

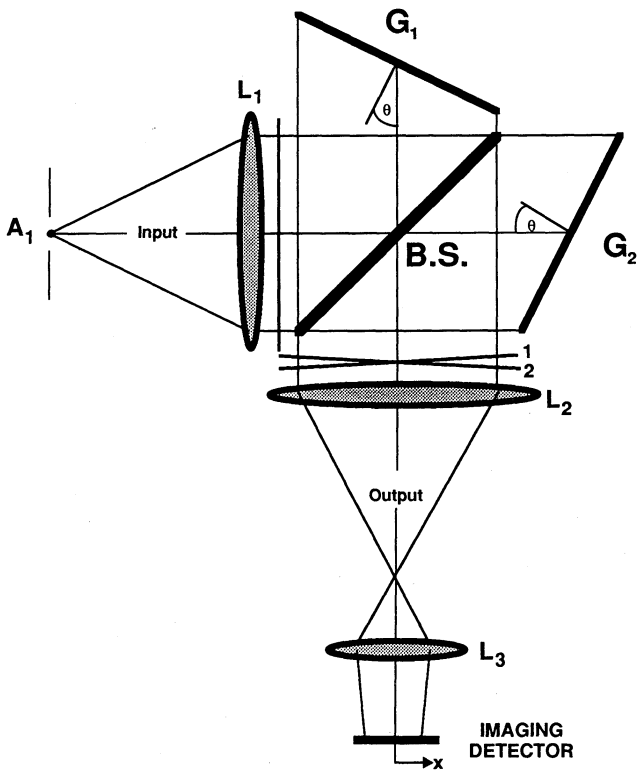

FIG. 1.—Schematic diagram of the basic SHS configuration. Wavelength-dependent Fizeau fringes which result from crossed wavefronts 1 and 2 at the exit of the interferometer are recorded along the x-direction by a position-sensitive detector. The Fourier transform of the fringe pattern recovers the spectrum.

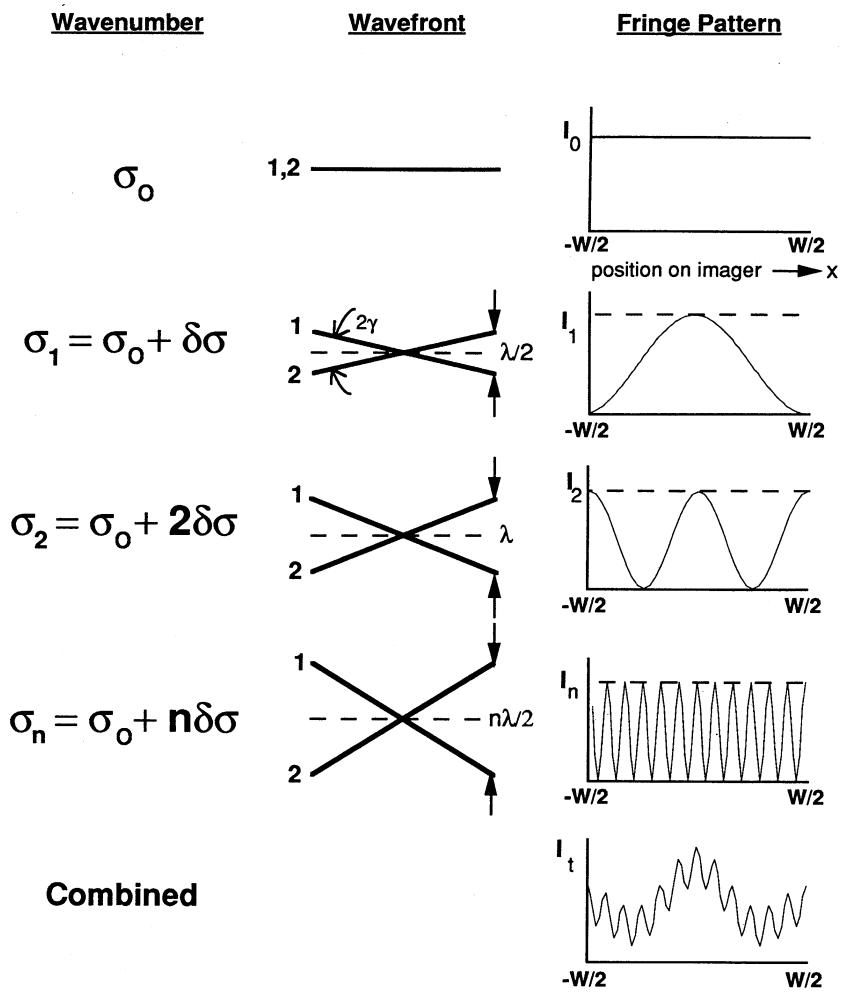

FIG. 2.—Relationship between wavenumber, wavefronts, and intensity patterns on the detector produced by SHS systems. The wavefronts are crossed at angles $2\gamma \simeq 4(1 - \sigma_0/\sigma) \tan \theta$, where σ_0 and θ are the Littrow wavenumber and grating angle, respectively (see text). In the second row a spectral line, having intensity I_1 and a wavenumber σ_1 that is $\delta\sigma$ from σ_0, produces crossed wavefronts with a maximum separation of $\lambda/2$ ($= 1/2\sigma_0$) at the edges of a detector of width W.

noise from the entire band effects each spectral element. Noise propagation in such multiplex systems has been studied extensively for FTS systems (Brault 1985; Mertz 1965; Baker 1977, for example), and this analysis can be readily adapted to SHS systems (Harlander 1991). The large body of literature describing FTS systems also describes the sensitivity of SHS systems with regard to other important experimental considerations. For example, the effects of detector nonlinearities, misalignment, thermal drifts, and scattered light on the recovered spectrum in SHS systems can be adapted from discussions of these experimental issues in the FTS literature.

One aspect where SHS differs markedly from FTS is with regard to the multiplex gain achieved by FTS systems when detector noise dominates the measurement. This gain is achieved by FTS systems because photons from all spectral elements are detected simultaneously on a single detector. The photon flux is increased by approximately the number of spectral elements detected; therefore, the detector noise is a smaller fraction of the total flux than it would be in a sequentially scanned system of comparable resolution. SHS systems record the entire interferogram simultaneously on a number of detector elements. Since the photon flux is spread out over a number of detector elements, the multiplex gain enjoyed by FTS in detector noise–limited situations does not apply to SHS. However, in the ultraviolet spectral region, the potential multiplex advantage of FTS is not realized anyway, because the detection is usually shot noise–limited.

The basic SHS system is similar to the SISAM interferometer (Connes 1958). SHS differs from the SISAM in that it uses an imaging detector to record all spectral elements simultaneously as opposed to the single channel scanned detection of the SISAM. The first description of a true SHS system was given by Dohi & Susuki (1971) who employed holographic film as the imaging detector. Advances in imaging detectors in the last decade have led to a rediscovery of the SHS concept both at the University of Wisconsin and in the Netherlands (Butcher et al. 1989). The thrust of the European effort has been to develop SHS for use with the next generation of large-aperture ($D \geq 8$ m) telescopes (Douglas, Butcher, & Melis 1990). At the University of Wisconsin, the thrust is the application of the technique for studies of diffuse emission lines originating from the interstellar medium and airglow. Our applications will use the full throughput advantage provided by SHS, including the development of field widening (§ 2.3., below).

2.2. *The Two-dimensional Spatial Heterodyne Spectroscopy Technique*

As can be seen from equation (3) and as has been demonstrated in earlier laboratory tests (Harlander & Roesler 1990), the symmetric heterodyned interferogram recorded by the SHS system described above leads to an ambiguity in the recovered spectra. The ambiguity is a result of the identical output for wavenumbers $+(\sigma - \sigma_0)$ and $-(\sigma - \sigma_0)$; hence, the recovered spectra are effectively folded about the point $\sigma = \sigma_0$. This ambiguity can be eliminated by using a two-dimensional format in the basic SHS system.

A two-dimensional interferogram is created by rotating one of the gratings in the basic system (Fig. 1) by a small angle, α, about an axis perpendicular to the optical axis and the grooves of the grating. This tilt breaks the symmetry of equation (3) by introducing a spatial modulation perpendicular to the modulation produced by the grating dispersion (eq. [2]). The fringes recorded by this system are no longer perpendicular to the x-axis; rather their orientation on the x-y plane (detector plane) is a function of the wavenumber of the incident light. The interferogram is then recast as

$$I(x, y) = \int_0^\infty B(\sigma)[\![1 + \cos\{2\pi[4(\sigma - \sigma_0)x \tan\theta + 2\alpha\sigma y]\}]\!]d\sigma . \quad (5)$$

For $\sigma = \sigma_0$, Fizeau fringes are recorded perpendicular to the y-axis with spatial frequency $f_y = 2\alpha\sigma$. Since f_y is a function of wavenumber, the interferogram along the y-dimension of the detector also represents a Fourier transform of the spectrum. Note that the spatial frequencies in the y-dimension are not heterodyned and the transform along y is therefore limited to low resolution. In addition to eliminating the ambiguity between $+(\sigma - \sigma_0)$ and $-(\sigma - \sigma_0)$, the two-dimensional format also allows the number of spectral elements that can be sampled without aliasing to be increased by a factor of 2 over that permitted by the one-dimensional format. The utility of this technique was demonstrated in some of the first laboratory spectra obtained with SHS (Roesler & Harlander 1991).

The spectral range can be increased even further if the gratings in Figure 1 are used in multiple orders. The resulting two-dimensional interferogram, with high resolution in one dimension (x) and low resolution in the other (y), is analogous to an echelle spectrogram. Then the system has a number of wavenumbers σ_{o_m}, one from each order m, which have $f_x = 0$ and are distinguished from each other by the low-resolution (cross-tilt) interferogram. From equation (1)

$$\sigma_{o_m} = \frac{m}{2d \sin\theta} . \quad (6)$$

The spectral range of a given order ($\Delta\sigma = 1/2d \sin\theta$) must be made small enough (i.e., f_x for light at the ends of the orders must be low enough) so that aliased signals are not produced as a result of undersampling by the N_x pixels along the x-dimension of the detector. The number of spectral elements within an order is thus limited to N_x. Furthermore, the cross-tilt angle α must be large enough so that the orders are resolved. This is achieved if the Littrow wavenumbers (eq. [6]) differ by at least one fringe in the y-dimension; that is, $\alpha \geq 1/2W_y\Delta\sigma$, where W_y is the grating width in the y-dimension. Complete separation of the orders along the y-dimension requires twice this tilt and restricts the number of orders that can be recovered unambiguously to $N_y/4$.

When the gratings in the SHS system are used in multiple orders, and the two-dimensional format is employed, the intensity distribution recorded on the imaging detector is given by

$$I(x, y) = \sum_m \int_0^\infty B(\sigma)d\sigma F_m(\sigma) \times [\![1 + \cos\{2\pi[4(\sigma - \sigma_{Om})x \tan\theta + 2\alpha\sigma y]\}]\!] , \quad (7)$$

where $F_m(\sigma)$ gives the blaze efficiency for order m. A two-dimensional Fourier transform of the Fizeau fringes produced by this device will then recover the echelle spectrograph format with high dispersion along x and low dispersion along y (see § 4.1.).

2.3. *Field Widening*

For spatially extended sources, an interference spectrometer is much more sensitive than a grating spectrometer of comparable area because it achieves a field-of-view solid angle that is typically two orders of magnitude greater than that achieved by the grating spectrometer at the same spectral resolution. The limitation on the field of view results from the change in path difference with off-axis angle. For Fabry-Perot and conventional FTS interferometers, the leading term in the expansion of path difference with respect to off-axis angle is quadratic, a dependence that arises solely from geometrical considerations. It is this quadratic dependence, as opposed to the linear dependence with conventional grating spectrometers, that gives interference spectrometers their basic throughput advantage.

In an effort to increase further the field-of-view gain of interference spectrometers, field-widening techniques have been developed for FTS systems (Baker 1977). Field-widened FTS (FW-FTS) systems achieve a field-of-view solid angle approximately two orders of magnitude greater than that of standard FTS, thus giving them a gain of four orders of magnitude over conventional diffraction grating systems. The increase in field of view can be used either to increase the sensitivity of the instrument (on sufficiently diffuse sources) or to decrease its overall size and cost. Field-widening techniques can also be applied to SHS systems (see §§ 2.3.2 and 4.2, below). The advantage of field-widened SHS (FW-SHS) systems over FW-FTS systems is that FW-SHS retains most of the characteristics of basic SHS systems (in particular, compact size and no moving parts) while achieving a field of view characteristic of FW-FTS systems.

2.3.1. *Field-widened Michelson Fourier Transform Spectroscopy*

Figure 3*a* illustrates the situation for the Michelson interferometer. The geometry implies that the path difference L' between the two arms for off-axis rays is related to the path difference L for axial rays by $L' = L\cos\phi \sim L(1 - \phi^2/2)$, where ϕ is the off-axis angle. The ϕ^2 term in this path difference can be eliminated by placing a material with refractive index n directly in front of the displaced mirror (Mertz 1965). A field-widened FTS system is illustrated in Figure 3*b*, where the thickness t of the refractive material is given by

$$t = \frac{nL}{2(n - 1)} . \quad (8)$$

The apparent geometric position of the mirrors now coincide when viewed from the exit aperture, while from a physical optics point of view, a path difference is retained. For this

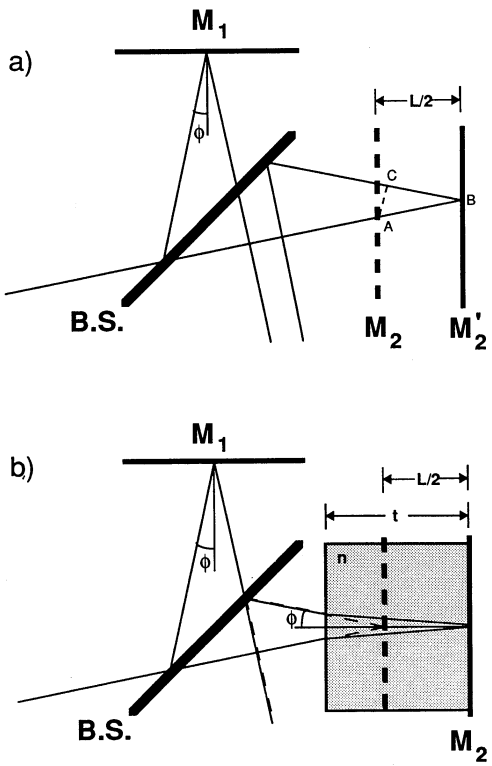

FIG. 3.—(*a*) Off-axis properties of a Michelson interferometer. When mirror at M_2 is moved to position M'_2, the path difference in the system becomes a function of off-axis angle ϕ. If the path difference for axial rays is L, as shown in the figure, then the off-axis path difference, denoted in the figure by $\overline{AB} + \overline{BC}$, is $L \cos \phi$. (*b*) Field-widened Michelson interferometer. When a material with refractive index n and thickness t is placed in front of the displaced mirror M'_2, the quadratic dependance on path difference with off-axis angle is eliminated. The thickness of the material is chosen so the geometric images of M_1 and M_2 appear coincident.

field-widened configuration the leading term in the path difference with off axis angle is ϕ^4 (Bouchareine & Connes 1963).

In order to construct a functioning field-widened FTS instrument, the thickness of the refractive material must be varied as the system is scanned (see eq. [8]), while at the same time achieving interferometric tolerances on the alignment of the scanned elements. Consequently, field-widened FTS instruments require complex scan and control mechanisms. Numerous instrumental configurations have been conceived in an effort to minimize the complexity associated with these devices, and many field-widened FTS interferometers have successfully operated in the field (Baker 1977).

2.3.2. *Field-widened Spatial Heterodyne Spectroscopy*

Field-widening techniques can be applied to SHS systems, but in marked contrast to field-widened FTS instruments, field-widened SHS instruments *have no moving parts*. The simplest field-widened SHS system is shown in Figure 4 where prisms P_1 and P_2 have been placed in the arms of the basic configuration of the device. The prism angle is selected so the diffraction gratings appear to be perpendicular to the optical axis and coincident when viewed at the output through the refractive material in the prisms. From a geometrical optics standpoint, the diffraction gratings behave as if they were mirrors in a conventional Michelson interferometer at zero path difference. Of course, at a sufficiently large off-axis, angle

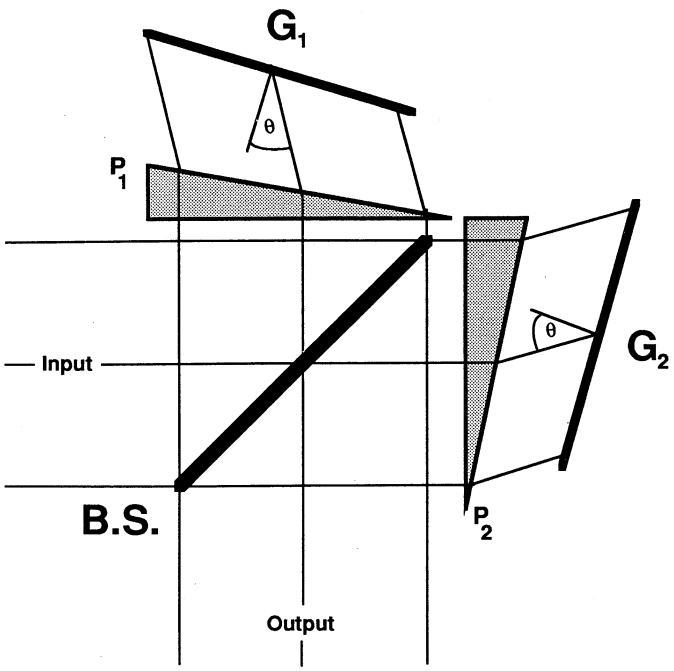

FIG. 4.—Field-widened SHS system. Prisms P_1 and P_2 are chosen so the diffraction gratings appear, from a geometrical optics point of view, coincident and perpendicular to the optical axis.

astigmatic aberrations introduced by the prisms will destroy the apparent geometric coincidence of the gratings but not before large gains are realized in many situations.

2.3.3. *Achromatic Field Widening*

For systems designed to cover a very broad spectral range (i.e., echelle mode; § 2.2., above), the chromatic dispersion of the prisms may present a problem. The effects of dispersion can be ameliorated to some extent by using achromatic prisms (Smith 1966) to perform field widening. The condition that must be satisfied for the prism to be achromatic at the wavenumbers σ_a and σ_b is given by

$$[n_1(\sigma_a) - n_1(\sigma_b)]\alpha_1 = [n_2(\sigma_a) - n_2(\sigma_b)]\alpha_2 , \qquad (9)$$

where n_i and α_i are the index of refraction and apex angle of prism i. A simple geometric argument demonstrates that, to first order, field widening can be accomplished by choosing prisms that are related to the grating angle θ by

$$\theta = \frac{n_1^2 - 1}{n_1}\alpha_1 - \frac{n_2^2 - 1}{n_2}\alpha_2 . \qquad (10)$$

Since the values of n_i are a function of wavenumber, equation (10) can be satisfied only at one particular wavenumber, σ_{FW}. For other wavenumbers, the field of view is decreased from the value at σ_{FW}. By choosing $\sigma_a < \sigma_{FW} < \sigma_b$, the benefits of the achromatic prism can be incorporated with minimal sacrifice in the field of view.

2.4. *Estimating the Signal-to-Noise Ratio Achieved by Spatial Heterodyne Spectroscopy Instruments*

The signal-to-noise ratio for detection of an emission line observed by SHS instruments with photon-limited detection is

given by

$$\frac{s}{n} = \frac{S}{2}\left[\frac{\epsilon A \Omega t}{f(S + B\Delta\lambda)}\right]^{1/2}, \quad (11)$$

where S is the signal strength of the emission line in photons $cm^{-2}\ s^{-1}\ sr^{-1}$, f is the number of spectral resolution elements per line width, B is the background continuum level in photons $cm^{-2}\ s^{-1}\ sr^{-1}\ Å^{-1}$, ϵ is the efficiency of the optical elements, Ω is the solid angle field-of-view, t is the integration time, and $\Delta\lambda$ is the spectral range admitted into the instrument (Harlander 1991). This equation does not include the effects of detector nonlinearities, distortions due to inaccurate flat fielding, grating scattering, vignetting, or chirping, but is adequate for estimating performance of SHS designed to measure the diffuse line emission from the interstellar medium (see § 5).

3. ALL-REFLECTION SPATIAL HETEODYNE SPECTROSCOPY CONFIGURATIONS

In spectral regions where transmitting optical elements are not available and highly reflective multilayer dielectric coatings have been developed, all-reflection SHS can be employed. The all-reflection configurations use a symmetrically ruled diffraction grating as the beam splitter/combiner and as a dispersive element in the system (Harlander 1991). The discussion here is limited to the one-dimensional format; however, except where indicated, the two-dimensional techniques addressed in § 2.2. are applicable to the all-reflection systems.

The simplest all-reflection configuration is shown schematically in Figure 5. Light enters the lower portion of the elliptical aperture S, is collimated by mirror M_3, and divided by beam-splitting grating G_0, which may be holographically produced to provide symmetric splitting. Mirrors M_1 and M_2, located symmetrically on either side of the grating, return the diffracted light to the grating, where the beams are recombined. The exiting beam is focused by mirror M_3 through the exit portion of the aperture and onto the imaging detector I. The diffraction grating acts both as the beam splitter and the dispersive element in the system. For a given wavenumber, the grating angle θ and the width of the grating W determine the resolving power of the simple all-reflection system; the result is $R = 4W\sigma \sin\theta$ (Harlander 1991). For a fixed resolving power, increasing the throughput by increasing the grating size requires decreasing θ. A practical limit is reached in the simple all-reflection system as θ is decreased because the instrument must be lengthened to provide clearance between the return mirrors for the incident and exiting light of G_0 (see Fig. 5). The overall size of the instrument can become large, especially for a low resolving power.

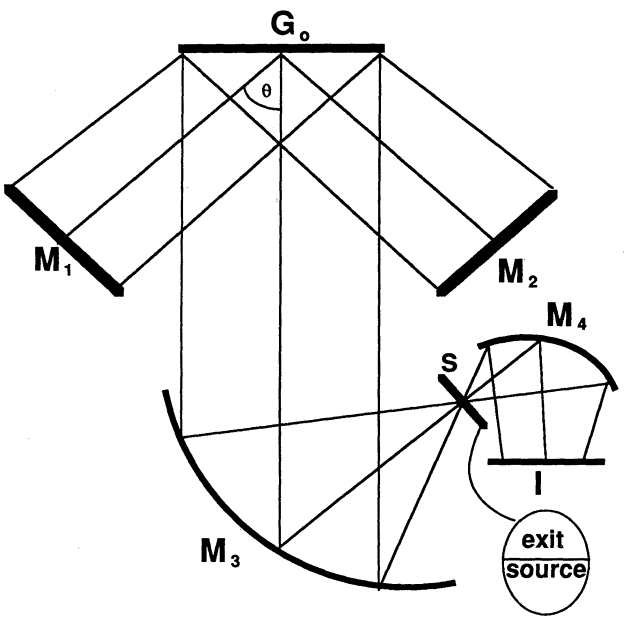

FIG. 5.—Schematic diagram of the all-reflection SHS configuration. Light enters the system through the lower half of split aperture S and exits through the upper half, after which it is imaged by M_4 onto an imaging detector I. The diffraction grating acts as both the beam splitter and dispersive element in the system.

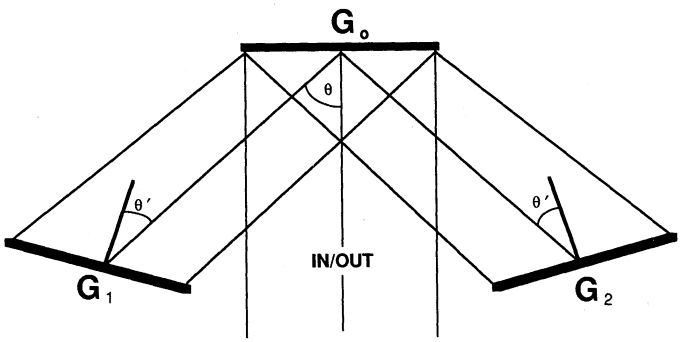

FIG. 6.—Reduced resolving power all-reflection SHS configration. Littrow gratings G_1 and G_2 cancel some of the path difference introduced by grating G_0. For a fixed resolving power, the angle θ is independent of the width of the gratings.

This limitation can be overcome by replacing the return mirrors in Figure 5 with matched diffraction gratings used in Littrow as shown in Figure 6. The beam-splitting grating can then be used at a relatively large angle because the path difference introduced by the beam-splitting grating is partly cancelled by the path difference introduced by the side gratings. If θ' is the Littrow angle of the side gratings, the maximum path difference L in this configuration is given by

$$L = 2W \sin\theta(1 - \tan\theta' \cot\theta), \quad (12)$$

which leads to a net resolving power of

$$R_0 = 4W\sigma \sin\theta(1 - \tan\theta' \cot\theta). \quad (13)$$

An off-axis analysis (Harlander 1991) shows that for these all-reflection configurations the field of view in the dispersion plane is reduced relative to the field of view in the basic SHS configuration (see § 2.1) by the factor cos θ. The field-of-view solid angle is thus also reduced by cos θ. It may be possible to field-widen an all-reflection SHS by employing reflective focusing elements in the arms of the interferometer (Harlander 1991). Such techniques have been applied successfully to FTS systems (Baker 1977); however, their application in SHS systems must currently be considered speculative since their practicality has not yet been demonstrated by careful analytic and laboratory studies.

A non–field-widened, all-reflection SHS has been assembled and tested in our laboratory at ultraviolet (i.e., 2500 Å) wavelengths (Harlander & Roesler 1990) and is presently being developed in collaboration with S. Chakrabarti at Berkeley for high-resolution planetary Lyman-alpha studies (Harlander et al. 1991).

4. PERFORMANCE TESTS AT VISIBLE WAVELENGTHS

In this section we describe the first proof-of-concept laboratory demonstrations of the two-dimensional, multiple-order (i.e. echelle) SHS system and the field-widened SHS configuration. Laboratory demonstrations of the more basic SHS concepts have been described previously by Harlander et al. (1991), Roesler & Harlander (1990), and Harlander & Roesler (1990).

4.1. *Tests of the Echelle Spatial Heterodyne Spectroscopy*

The spectrum of a mercury discharge lamp was obtained with a broad-band, two-dimensional SHS system similar to Figure 1 with the exception that one of the gratings was replaced by a plane mirror in order to minimize the cost of the spectrometer. This system has properties that are identical to the system described in § 2.2, except that the resolving power is reduced by a factor of 2 from that given in equation (4), because with a single grating, the total path difference is halved. In practice, a two-grating system is desirable for low light level astronomy because it provides some degree of self-filtering by diffracting unwanted light away from the optical axis and thus away from the detector. The grating in the system had a blaze angle of approximately 13°.9 and a groove density of 20 lines mm^{-1}. Approximately 8 by 8 mm of the grating was imaged onto a 2.64 by 2.64 mm CCD detector with a 165 by 192 pixel format. Light was detected in orders 41 through 56, corresponding to a wavenumber range of approximately 17,000 cm^{-1} to 23,200 cm^{-1}.

The mercury spectrum was chosen for the test of the echelle mode because in the visible portion of the spectrum mercury is comprised of a few, well-known emission lines. The cross-tilt angle α (see § 2.2.) was set to approximately 12′ so that the highest wavenumber we detected in the mercury source (σ = 22,945 cm^{-1}) produced approximately 63 fringes along the y-dimension of the detector. Figure 7 shows the interferogram recorded by the CCD detector in our test system. The dispersion plane of the grating is along a horizontal slice through the image. The predominant set of fringes whose crests run from 11 o'clock to 5 o'clock are attributed to the strong 18,312.6 cm^{-1} (λ5461) mercury line; fainter fringes associated with other lines can be seen at other angles. Figure 8 shows a portion of the two-dimensional Fourier transform of the pattern recorded by the detector. High dispersion is along the axis labeled spatial frequency and low dispersion along the order axis. Four lines are detected with a recorded intensity ratio of 7.5 between the faintest and brightest line. All of the lines are far above the noise floor. Identifying the lines labeled a and b on the figure as 18,312.6 cm^{-1} and 17,332.3 cm^{-1}, respectively, and using them to calibrate the field, we can calculate the wavenumbers of the other prominent features in the image. The results of these calculations are shown along with accepted values in Table 1. The accuracies obtained are consistent with the resolution of the system ($\delta\sigma$ = 2.61 cm^{-1}). The performance of this system confirms the broad-band echelle mode capabilities that had been predicted by the earlier analytic studies (Harlander 1991).

TABLE 1

MERCURY EMISSION LINES MEASURED BY AN ECHELLE SPATIAL HETERODYNE SPECTROSCOPY

	ACCEPTED VALUE		MEASURED BY SHS	
LINE	Wavelength (Å)	Wavenumber (cm^{-1})	Grating Order	Wavenumber (cm^{-1})
a.....	5461	18,312.6	44	Calibration
b.....	5770	17,332.3	42	Calibration
c.....	5790	17,270.6	42	17,269
d.....	4358	22,944.6	55	22,943

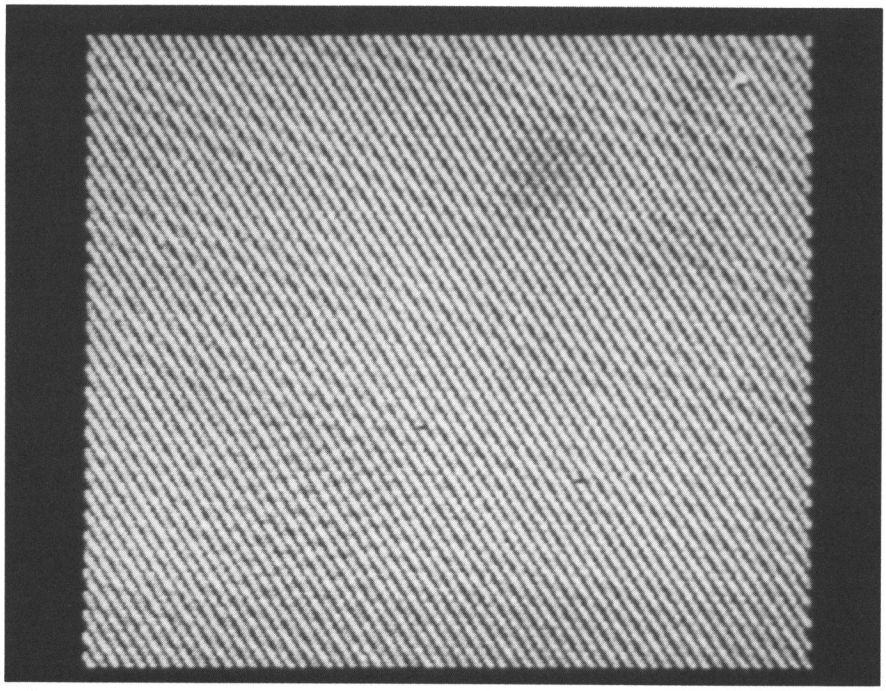

FIG. 7.—Mercury interferogram produced by the echelle SHS system. The dispersion plane of the grating is along a horizontal slice through the image.

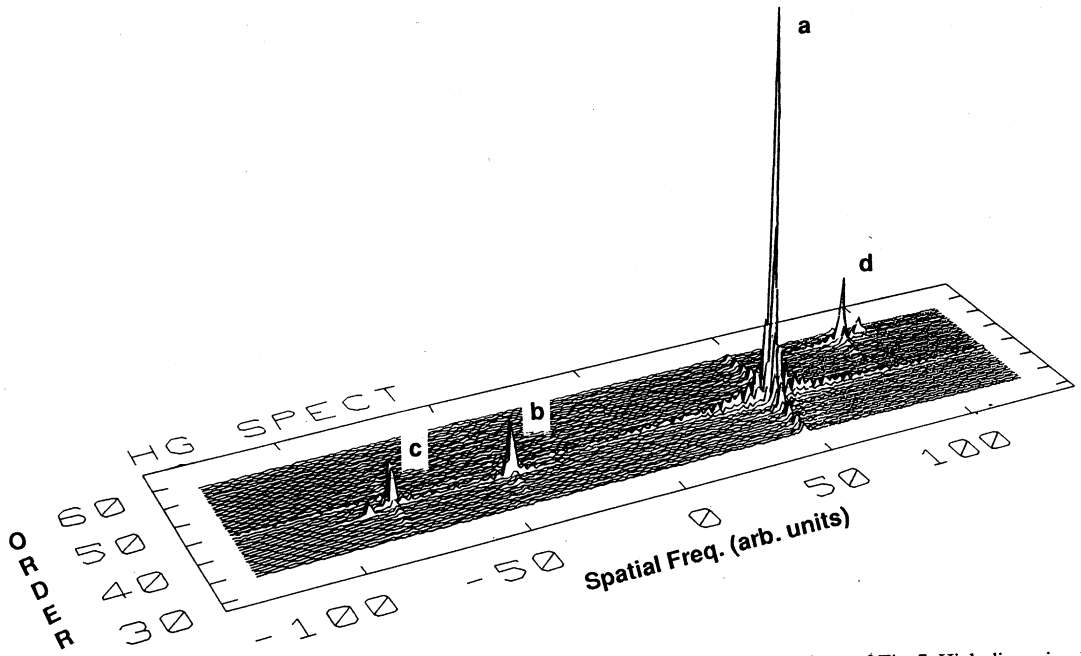

FIG. 8.—Visible mercury spectrum measured by the echelle SHS system; the two-dimensional Fourier transform of Fig. 7. High dispersion is along the *spatial frequency* axis; the low-dispersion axis, labeled *order*, gives the approximate grating order. Identification of lines labeled a and b calibrates the entire wavenumber field. The calculated wavenumbers and accepted values for lines c and d are given in Table 1. The ringing in the wings of the bright lines is the result of the finite range of the interferogram and represents the unapodized instrumental profile of the system.

4.2. *Tests of a Field-widened Spatial Heterodyne Spectroscopy*

The field-widened SHS system (Fig. 4) was tested using two matched gratings with 1200 lines mm^{-1} and prisms appropriate for field widening at the Hα line (λ = 6563 Å). The angle θ for these gratings at Hα is 22°.3, and the optical index of the prism is n = 1.5143 at Hα, which determines the angle required for field widening as 27°.1 (Harlander 1991). The Hα line produced by our discharge lamp was unresolved by the spectrometer, which had a resolving power of 20,000. The spatial frequency of the fringes produced by this system were measured as a function of off-axis input angle in order to determine the maximum solid angle permitted by this field-widened system. The maximum field of view is reached when the spatial frequency of the fringes produced by the off-axis rays differs from the on-axis spatial frequency by an amount equal to the spectral resolution of the system.

The results of these tests are shown in Figure 9, in which the measured change in spatial frequency (expressed as wavenumber) with off-axis angle is plotted for angles along the dispersion plane of the gratings and perpendicular to this plane. The solid lines on the figure are theoretical values (from Harlander 1991) for the wavenumber shift with off-axis angle for three cases: a non–field-widened system (e.g., a Fabry-Perot or standard Michelson interferometer), our field-widened SHS system in the dispersion plane of the gratings, and our field-widened SHS system perpendicular to the dispersion plane. The dashed curve gives the calculated wavenumber shift with angle perpendicular to the dispersion plane given that in our test system; there was a 5′ angular mismatch between the grating angle and the prism angle appropriate for optimum field widening. Our measured values for the wavenumber change with off-axis angle are also shown in the figure. The triangles correspond to angles parallel to the dispersion plane and the boxes are for measurements in the perpendicular direction. Open and closed symbols indicate measurements on opposte sides of the optical axis. The measured values are consistent with the predicted values parallel to the dispersion plane. Perpendicular to this plane, the field of view of our field-widened SHS is slightly less than the maximum predicted from the analytical studies (*dashed curve*). This discrepancy is believed to be a result of slight misalignments of the prisms in the arms of the interferometer in our test system. More accurate alignment procedures are now being developed.

Our system achieves a field of view perpendicular to the dispersion plane that is over an order of magnitude larger than the field for a conventional (non–field-widened) Fabry-Perot

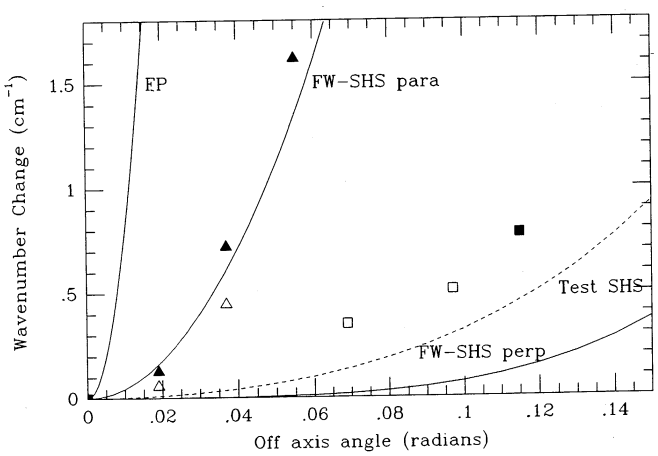

FIG. 9.—Wavenumber change as a function of off-axis angle for our field-widened SHS system. FP: expected variation for a Fabry-Perot or standard Michelson interferometer; FW-SHS para: expected variation parallel to the dispersion plane for the field widened SHS; FW-SHS perp: expected variation perpendicular to the dispersion plane for the field widened SHS; Test SHS (*dashed curve*) expected variation perpendicular to the dispersion plane for our test system given the angular mismatch between the prism and grating angles. Measurements parallel to the dispersion plane are denoted by triangles and perpendicular by squares. Open and filled symbols denote measurements on opposite sides of the optical axis.

or Michelson interferometer. The total gain in solid angle due to field widening is a factor of 50. The asymmetry in the field of view, evident in the measurements and predicted by the analytical studies, is due to aberrations introduced by the relatively large prism angle used in our system (Harlander 1991). This angle was dictated by our use of off-the-shelf gratings purchased for an entirely different purpose. For the more modest prism angles that would be used in a custom SHS system, the aberrations are reduced and the field of view in the dispersion plane of the gratings approaches the field of view perpendicular to the dispersion plane.

5. SPATIAL HETERODYNE SPECTROSCOPY FOR THE FAR-ULTRAVIOLET

5.1. *Scientific Motivation*

The goal of the Wisconsin field-widened SHS development (§§ 2 and 4) is to obtain velocity-resolved, all-sky maps of the interstellar line emission in the spectral region 1350–1950 Å (Roesler et al. 1990). The recent discovery by Martin & Bowyer (1990a) of faint, diffuse line emission at high Galactic latitudes has opened up an important new window on the interstellar medium. These observations, made with a Rowland spectrograph on the Berkeley Extreme Ultraviolet/Far-Ultraviolet Shuttle Telescope (shuttle mission 61-C), clearly revealed C IV λ1550 and O III] λ1663 emission from 10^5 K gas in the diffuse interstellar medium. Other lines may be present as well within the 1400–1900 Å band. The C IV data in the half-dozen widely spaced directions that it was detected suggest that the emission is from an extended source that covers the sky and is absorbed at low Galactic latitude by interstellar dust near the Galactic midplane. The observed intensity of the C IV doublet ranges from about 3000 to 6000 photons cm^{-2} s^{-1} sr^{-1}, while the background continuum intensity ranges from 300 photons cm^{-2} s^{-1} sr^{-1} $Å^{-1}$ at high Galactic latitude to 1500 photons cm^{-2} s^{-1} sr^{-1} $Å^{-1}$ near the Galactic midplane.

The nature of hot (10^5–10^6 K) gas, long thought to play a dominant role in the interstellar medium, is the subject of much debate. For recent reviews and discussions, see McKee (1990), Spitzer (1990), Cox (1989), and McCammon & Sanders (1990). Hot interstellar gas is generally believed to be produced by high-velocity shocks from supernova remnants, which expand into the ambient medium and create hot, low-density bubbles, 50–100 pc in radius. If these bubbles are long-lived and are created frequently enough, they will profoundly influence the structure and dynamics of the interstellar medium by interconnecting and occupying most of the interstellar volume (Cox & Smith 1974; McKee & Ostriker 1977). Buoyant forces could also carry the gas far from the Galactic midplane, producing a hot Galactic corona (Spitzer 1956) and large-scale vertical motions (Shapiro & Field 1976). To be sure, the existence of hot interstellar gas was confirmed years ago with the detection of ultraviolet absorption lines (Jenkins & Meloy 1974) and diffuse soft X-ray emission (Bowyer, Field, & Mack 1968; Williamson et al. 1974) from highly ionized trace elements within the interstellar medium. However, its pervasiveness and influence on the structure and motions of the medium has not yet been established. In fact, a rethinking of some of the original assumptions has put the theoretical basis for the existence of a *pervasive* hot component in doubt (Cox 1989; Slavin & Cox 1992).

This uncertainty about such an important astrophysical question is due in large part to the fact that until now no practical spectroscopic technique existed that could provide radial velocity–resolved maps of the emission lines. Such maps are necessary in order to understand the distribution and kinematics of the gas and its relationship to the other, cooler components of the medium. As pointed out by Heiles (1991) in his review of the observational aspects of the interstellar disk-halo connection in our Galaxy, "If this [10^5 K] gas is truly globally distributed within the Galaxy, it will be one of the most important components of the ISM from the standpoint of energetics and hence, theoretical significance. Clearly more extensive observations are required."

The development of high-throughput SHS techniques now provides a unique opportunity to study the FUV emission lines at high spectral resolution (20 km s^{-1}) and thus to explore in detail the kinematics, distribution, and ionization/excitation conditions of 10^5 K gas over the sky and throughout a large section of the Galactic disk and halo. An FUV SHS also opens up the possibility of high spectral resolution studies of molecular hydrogen fluorescence emission, produced by UV radiation that penetrates cold H_2 clouds (Martin & Bowyer 1990b).

5.2. *Performance Predictions*

The visible light performance tests described in § 4 allow us to predict with some confidence the performance of an SHS device for the interstellar FUV application. Since C IV λ1548,51 are the brightest lines (Martin & Bowyer 1990a), we describe below the ability of SHS to produce a radial velocity–resolved map of the high Galactic latitude C IV emission. The source is assumed to be comprised of lines of intensity 2600 photons cm^{-2} s^{-1} sr^{-1}, which is the expected mean intensity of the brighter C IV λ1548 line in the doublet at $|b| \gtrsim 35°$ (Martin & Bowyer 1990a). The background continuum is 600 photons cm^{-2} s^{-1} $Å^{-1}$, which represents the average continuum intensity at $|b| = 40°$ (Bowyer 1991). The proposed system for a survey of this emission is a field-widened SHS employing UV-quartz and MgF_2 optics and a prefilter to reduce photon noise due to the background continuum. The detector is assumed to be a photon-counting array with a CsI photocathode and quantum efficiency 0.15. The prefilter is a commercially available all-dielectric narrow-band filter (Zuckic et al. 1990). Such a filter designed for the C IV survey achieves a peak transmission of 60%, bandpass 70 Å, and field of view 15° × 15° (M. Zuckic, private communication). The SHS system is comprised of gratings 5 × 5 cm with groove density 150 lines mm^{-1} operated at a blaze angle of 0.°7 in first order. The resolving power is 15,000. Computer modeling of this system indicates that, in principle, it can achieve a field of view in excess of 20° × 20°. Our proposed system, however, will have a 15° × 15° field for compatibility with the prefilter. A more desirable angular resolution of 3° on the sky would require coupling the system to a 25 cm diameter primary mirror. The assumed efficiencies of the optical elements are 0.7 for the beamsplitter, 0.8 for each mirror, 0.8 for each field-widening prism, and 0.4 for each grating.

For this SHS system to detect a C IV λ1548 line two spectral elements, or 40 km s^{-1}, wide (Savage & Massa 1987) with an average signal-to-noise ratio of 15, which is sufficient to obtain information on the shape of the line profile as well as its radial velocity, equation (11) predicts that the required integration time is 40 minutes for each angular resolution element on the sky. For an observation efficiency of 25%, an all-sky, velocity-resolved map consisting of the 2900 angular resolution ele-

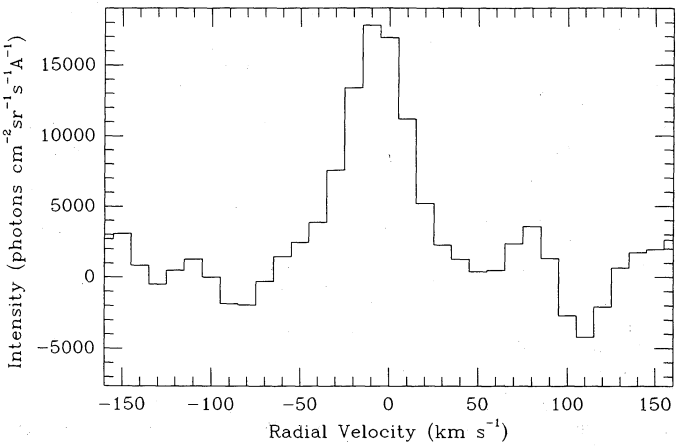

FIG. 10.—Results of a simulation of a narrow-band SHS sounding rocket observation of interstellar C IV emission. Shown is the velocity-resolved ($\lambda/\delta\lambda = 15{,}000$) 1548 Å C IV line (a Gaussian 40 km s^{-1} FWHM) after a 5 minute integration. The other line of the doublet at +500 km s^{-1} is outside the limited radial velocity range of this figure; however, both lines would be recorded by the SHS spectrometer.

ments for $|b| \geq 30°$ could be obtained in less than 1 yr, the lifetime of a small explorer satellite.

For a sounding rocket demonstration of SHS, equation (11) predicts a signal-to-noise ratio of 10 could be obtained in 5 minutes for the brighter line of the doublet in a direction of relatively high C IV intensity and low background, Martin & Bowyer's directions 1 and 8. Figure 10 shows the result of a numerical simulation of the C IV λ1548 spectrum obtained with such a narrow-band SHS instrument. A synthetic interferogram was generated assuming an integration time of 5 minutes on a source comprised of two lines of intensity 3300 and 1600 photons cm^{-2} s^{-1} sr^{-1} and a background continuum of 300 photons cm^{-2} s^{-1} sr^{-1} Å^{-1}, appropriate for direction 1. Poisson noise was added before transforming. The signal-to-noise ratio of the line in the transform is approximately 10, thus confirming the predictions of equation (11).

As another figure of merit for SHS, we compare the calculated grasp (effective area times field of view product $\epsilon A\Omega = 5.0 \times 10^{-3}$ cm^2 sr) of the field-widened, high-resolution (15,000) SHS system with that of the relatively low resolution (100) grating spectrograph on the Berkeley EUV/FUV Shuttle Telescope ($\epsilon A\Omega = 1.2 \times 10^{-4}$ cm^2 sr at 1500 Å), the instrument that discovered the diffuse C IV emission. The grasp of the SHS is a factor of 40 larger *with 150 times the spectral resolution.* The SHS system requires approximately 1/12 the integration time, however, because photon noise propagates differently in the two systems; that is, SHS is a true multiplex device in which photon noise from the entire band affects each spectral element.

We point out that the SHS we have considered here uses only 5 × 5 cm gratings, compared, for example, to the 15 × 15 cm grating of the Berkeley spectrometer. We chose this size for the SHS because it is the size of the system we have actually built and tested at visible wavelengths. Also, while there is no technical limitation to larger gratings for an SHS, it is not yet certain that for the FUV, the field-widening wedges and beam splitter can be made much larger than 5 cm and still retain the required interferometric quality. If a 15 cm SHS system can be built, then the resulting throughput of the SHS will be an order of magnitude larger than that discussed above, with a corresponding reduction in the required integration times.

The above performance predictions do not include the effects of stars with significant FUV fluxes that fall within the field of view. Such stars can be avoided in the sounding rocket measurements by choosing an appropriate observation direction at high Galactic latitude. For the survey instrument, the photons from these stars could be removed by imaging the sky on the fringe plane and time-tagging each photon as the field of view of the instrument drifts across the sky. An interferogram of each part of the sky could then be reconstructed, excluding the small regions contaminated by the stellar images.

6. CONCLUSIONS

We have conceived and demonstrated a new technique for interference spectroscopy, called spatial heterodyne spectroscopy (SHS), which is suitable for the study of faint, diffuse emission lines at any wavelength. SHS has no moving parts, can be field-widened for an additional factor of 100 increase in throughput over that of standard interferometric systems ($\times 10^4$ over conventional grating spectrometers), and can be constructed in all-reflection configurations. We believe that this new instrumental approach has broad possibilities for driving major scientific advances in several areas of astrophysics, particularly at wavelengths shorter than 2000 Å, where the full advantages of interference spectroscopy have not been realized.

SHS is currently being investigated for its competitiveness with traditional grating spectrometers in the FUV; however, studies of SHS should be expanded to discover additional areas where it may be superior to conventional techniques. For example, continuing improvements in dielectric multilayer coatings for diffraction gratings (e.g., Ritva et al. 1990) offer the possibility of extending all reflection SHS configurations into the EUV.

We gratefully acknowledge the valuable assistance provided by Gabriel Li, who was very much involved with the alignment and testing of the field-widened SHS. We also acknowledge support for this work from the National Aeronautics and Space Administration through grants NAG5-674 and NAGW-1861 and support from the National Science Foundation through grant AST 88-13467.

F. L. R. gratefully acknowledges National Science Foundation support through an independent research agreement while serving as Program Director for Aeronomy in the Division of Atmospheric Sciences.

REFERENCES

Baker, D. 1977, Spectrometric Techniques, vol. 1 (New York: Academic), 71
Bouchareine, P., & Connes, P. 1963, Le Journal de Physique et le Radium, 24, 134
Bowyer, C. S. 1991, ARA&A, 29, 59
Bowyer, C. S., Field, G. B., & Mack, J. E. 1968, Nature, 217, 32
Brault, J. W. 1985, High Resolution in Astronomy: Fifteenth Advanced Course of the Swiss Society of Astronomy and Astrophysics, ed. A. Benz, M. Huber, & M. Mayor (Sauverny: Geneva Observatory), 1
Butcher, H., Douglas, N., Frandsen, S., & Maaswinkel, F. 1989, High Resolution Fourier Transform Spectroscopy, 1989 Technical Digest Series, vol. 6 (Washington, DC: Optical Society of America), 9
Connes, P. 1958, Le Journal de Physique et le Radium, 19, 215
Cox, D. P. 1989, in IAU Colloq. 120, Structure and Dynamics of the Interstellar Medium, ed. G. Tenorio-Tagle, M. Moles, & J. Melnick (New York: Springer-Verlag), 500
Cox, D. P., & Smith, B. W. 1974, ApJ, 189, L105

Dohi, T., & Suzuki, T. 1971, Appl. Opt., 10, 1137
Douglas, N. G., Butcher, H. R., & Melis, M. A. 1990, Ap&SS, 171, 307
Fonck, R. J., Huppler, D. A., Roesler, F. L., Tracy, D. H., & Daehler, M. 1978, Appl. Opt., 17, 1739
Harlander, J. M. 1991, Ph.D. thesis, Univ. of Wisconsin-Madison
Harlander, J., & Roesler, F. L. 1990, in Instrumentation in Astronomy VII, ed. D. L. Crawford (Proc. SPIE, 1235), 622
Harlander, J., Roesler, F. L., & Chakrabarti, S. 1991, in X-Ray-EUV Optics for Astronomy, Microscopy, Polarimetry, and Projection Lithography, ed. O. Siegmund (Proc. SPIE, 1344), 120
Heiles, C. 1991, in IAU Symp. 144, The Interstellar Disk-Halo Connection in Galaxies, ed. H. Bloemen (Dordrecht: Kluwer), 433
Jenkins, E. B., & Meloy, D. A. 1974, ApJ, 193, L121
Kruger, R. A., Anderson, L. W., & Roesler, F. L. 1972, J. Opt. Soc. Am., 62, 938
Martin, C., & Bowyer, S. 1990a, ApJ, 350, 242
———. 1990b, ApJ, 354, 220
McCammon, D., & Sanders, W. T. 1990, ARA&A, 28, 657
McKee, C. F. 1990, in The Evolution of the Interstellar Medium, ed. L. Blitz (ASP Conf. Ser., 12), 3
McKee, C. F., & Ostriker, J. P. 1977, ApJ, 218, 148
Mertz, L. 1965, Transformations in Optics (New York: Wiley)
Reynolds, R. J. 1990, in IAU Symp. 139, Galactic and Extragalactic Background Radiation, ed. S. Bowyer & C. Leinert (Dordrecht: Kluwer), 157
Reynolds, R. J., Roesler, F. L., Scherb, F., & Harlander, J. 1990, in Instrumentation in Astronomy, ed. D. Crawford (Proc. SPIE, 1235), 610
Ritva, A. M., Keski-Kuuha, Thomas, R. J., Gum, J. S., & Condor, C. E. 1990, Appl. Opt., 29, 4529
Roesler, F. L. 1974, in Methods Exper. Physics, 12, A, 531
Roesler, F. L., & Harlander, J. 1991, in Optical Instrumentation for the 1990s: Applications in Astronomy, Chemistry, and Physics, ed. B. J. McNamara (Proc. SPIE, 1318), 234
Roesler, F. L., Harlander, J., & Reynolds, R. J. 1990, in IAU Coll. 123, Observations from Earth Orbit and Beyond, ed. Y. Kondo (Dordrecht: Kluwer), 481
Roesler, F. L., Reynolds, R. J., Scherb, F., & Ogden, P. M. 1978, in High Resolution Spectroscopy, Proc. 4th Colloq. on Astrophysics of the Trieste Observatory, ed. M. Hack (Trieste: Osservatorio Astronomico di Trieste), 600
Savage, B. D., & Massa, D. 1987, ApJ, 314, 380
Shapiro, P. R., & Field, G. B. 1976, ApJ, 205, 762
Slavin, J. D., & Cox, D. P. 1992, ApJ, 392, 131
Smith, W. J. 1966, Modern Optical Engineering: the Design of Optical Systems (New York: McGraw Hill)
Spitzer, L., Jr. 1956, ApJ, 124, 20
———. 1990, ARA&A, 28, 71
Stroke, G. W., & Funkhouser, A. 1965, Astrophys. Lett., 16, 272
Williamson, F. O., Sanders, W. T., Kraushaar, W. L., McCammon, D., Borken, R., & Bunner, A. N. 1974, ApJ, 193, L133
Zukic, M., Torr, D. G., Spann, J. F., & Torr, M. R. 1990, Appl. Opt., 29, 4293